Fixed Pattern Correction and Rapid Analysis Procedures for He I 1083 nm Imaging Spectroscopy with the NASA/NSO Spectromagnetograph

Harrison P.Jones (hjones@noao.edu)
NASA's Goddard Space Flight Center

Abstract. Imaging spectroscopy in the He 1083 nm lines is a powerful tool for probing the top of the chromosphere and bottom of the transition region. A method for spectral flat-fielding using a uniform solar exposure with spectral lines in place is presented and illustrated with 1083 nm data obtained with the NASA/NSO Spectromagnetograph at the National Solar Observatory Kitt Peak Vacuum Telescope. An efficient method for analysis of the data producing images in continuum intensity, line-of-sight velocity, equivalent width, central line depth, Doppler width, and line asymmetry is also presented and illustrated.

1. Introduction

Solar Helium lines have been the object of intense study since their observation in eclipse spectra (Janssen, 1868) led to the discovery of Helium as a chemical element. Current observational interest stems from the fact that thermodynamic conditions favorable for the formation of this inert gas exist only in a narrow region of the outer chromosphere and cool transition region so that the temporal and spatial variations of the He lines provide unique and valuable information on the structure and dynamics of the outer solar atmosphere. However, models of the solar line formation for Helium still fail to explain important aspects of the observations so that physical interpretation of the data is correspondingly uncertain. For example, the relative roles of collisional and photoionization-recombination processes are still debated (Andretta and Jones, 1997; Andretta, Del Zanna, and Jordan, 2003), and averaged hydrostatic and statistical equilibrium models of the chromosphere and transition region which predict the strengths of most other transition region lines underestimate the strengths of the helium lines (Jordan, 1975; Jordan, Macpherson, and Smith, 2001).

Imaging spectroscopy (i.e., the collection of resolved spectra at every spatial point within an extended field of view) from scanning spectrographs and tunable filters is a relatively recent tool which is providing new insights and constraints on models of He formation and new information about the solar atmosphere. Examples of studies from spacecraft imaging spectroscopy include the full-disk reconstruction

of He I 58.4 nm spectra by Peter (1999) from SOHO/SUMER data and the comparison of spatially resolved He I resonance line emission with differential emission measure from other EUV transition lines by Jordan, Macpherson, and Smith (2001) using SOHO SUMER and CDS data. Research derived from ground-based imaging spectroscopy includes polarimetric studies of the He I 1083 nm and nearby lines by Lin, Penn, and Kuhn (1998) using the Horizontal Spectrograph at the NSO/SP Dunn Vacuum Tower Telescope and by Solanki *et al.* (2003) using the Tenerife Infrared Polarimeter at the Vacuum Tower Telescope of the Observatorio del Teide. Similarly, Schmidt, Muglach, and Knölker (2000) identified a high-velocity free-fall event in time series of long-slit spectra using the German VTT on Tenerife. Penn and Jones (1996) and Dupree, Penn, and Jones (1996) used imaging spectroscopy from the NASA/NSO Spectromagnetograph (SPM) at the NSO/Kitt Peak Vacuum Telescope to study He I 1083 nm limb emission and line asymmetry in coronal holes, respectively.

In spite of this progress, however, the 1083 nm line remains difficult to analyze accurately and in detail for three principle reasons. First, it is typically weak with central depths usually only a few percent of the continuum. Random or systematic errors which are small compared to the continuum thereby become important or even dominant sources of error for the line profile. Second, the line is highly variable in both space and time so that it is difficult to devise a single reduction algorithm which works reliably for all the conditions likely to be encountered during an observation. Finally, the line is blended in highly varying proportions with a nearby solar Si I line to the blue and a blend of Telluric water vapor and solar lines to the red. Thus it is difficult to specify the continuum from the data, a task that ideally demands a stable detector with a large spectral range ($\sim$ 20 Å). As a step toward improving the physical reliability and interpretability of He I 1083 nm imaging spectroscopy, this paper concentrates on flat-fielding and rapid analysis techniques applied to data obtained by the SPM.

2. Instrument and Data

The SPM (Jones *et al*, 1992) is mounted at the focal plane of the Littrow spectrograph of the NSO/Kitt Peak Vacuum Telescope (KPVT). Anamorphic optics with approximately 3:1 spatial:spectral demagnification reimage a 512 arc-sec by $\sim$ 2 nm section of the long-slit exit spectrum onto a CCD which is read out in frame-transfer mode at video rate. The spectrum is oriented with the spatial dimension parallel to the camera read-out direction so that any systematic read patterns are

perpendicular to the dispersion—a characteristic that is of some advantage in fixed-pattern removal as will be discussed below. A special data system built with commercial off-the-shelf components digitizes the video signal synchronously with the pixel-by-pixel read out, sorts video fields by polarization state, and accumulates the spectra either for real-time analysis by a board-level computer or for storage on disk. Imaging spectroscopy is achieved by scanning the telescope's solar image across the entrance slit of the spectrograph.

In second order at 1083 nm, a CCD pixel spans 1.14 arc-seconds in the direction of the entrance slit and 8.39 pm in wavelength. For full-disk synoptic observations, the accumulation time of the video readout is set at 9 video frames (0.3s) and the image is scanned at 3.8 arc-second/s so that the effective spatial pixels are square. For special observations of limited areas, the accumulation time is typically four times longer and the scanning rate is four times slower so that the data achieve about twice the signal-to-noise ratio of the synoptic observations. When higher time resolution is desired, the accumulation time and scan rate are often adjusted for two or three times coarser resolution and/or lower signal-to-noise ratios. The detector is a silicon TI CCD mounted in a COHU television camera with fan-driven flow of room-temperature air but no active thermal control. The SPM has been in daily operation since April, 1992 and will soon be replaced by the new Vector Spectromagnetograph (VSM) of the Synoptic Optical Long-Term Investigations of the Sun (SOLIS) project. The VSM will also be capable of imaging spectroscopy at 1083 nm with a much improved detector and camera but with about half the spectral range of the SPM.

An example of an unprocessed long-slit spectrum obtained with the SPM is shown in the top panel of Figure 1. The bottom panel shows the data after dark-current subtraction and fixed-pattern removal (flat-fielding), processes which will be discussed in detail in the next section since they strongly affect the analysis of He I 1083 nm spectra. The spectra in Figure 1 are shown in the camera's frame of reference; i.e., the entrance slit, which is usually oriented to be parallel to heliographic north-south on the solar image, is always projected to be parallel with camera rows while wavelength variation is parallel to camera columns. Several rows at both the top and bottom of the imaged spectra never contain useful solar data, and image stops at the left and right are governed by the collimator lens of the reimaging system and the edge of the camera. The data are trimmed to a rectangular subarray filled with useful data before analysis.

For daily full-disk synoptic observations, the spectra are analyzed in cadence with the scanning of the solar image using a simple algorithm

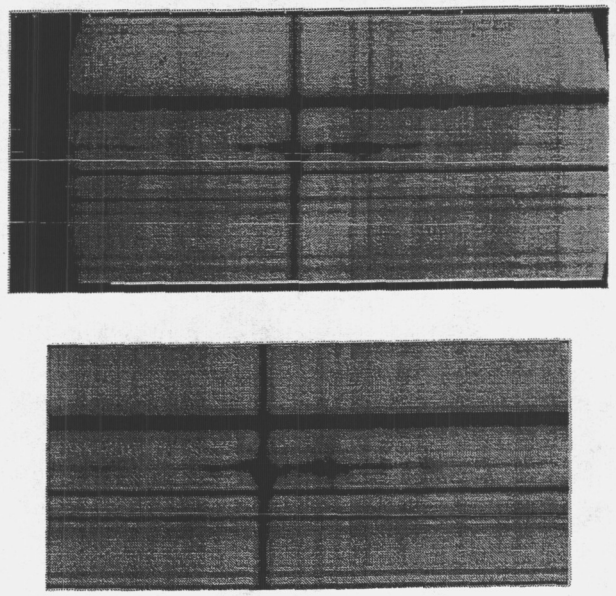

Figure 1. Sample raw and flat-fielded long-slit spectrum from the SPM. Data were obtained on 1999 November 9. Slit direction is horizontal and dispersion is vertical. The dark vertical feature is a sunspot.

(see Jones *et al.*, 1992) to calculate intensity and equivalent width; the original spectra are not saved. The full-disk equivalent width for 99 November 9 is shown in Figure 2 with negative contrast so that areas where the line absorbs strongly appear dark and coronal holes, where the line is very weak, appear bright by comparison. For special observations called a "zone area scans" the raw spectra are stacked into large data cubes and saved as 3D FITS files with no real-time processing. In the following section, the analysis of such a zone area scan is illustrated for spectra obtained on 99 November 9 within the outlined area in Figure 2. The spectrum of Figure 1 was selected from this observation.

3. Spectral Flat-Fielding

To remove detector and optical artifacts from SPM spectra, we follow customary practice and assume that a straight line describes the exposure response for each pixel. Thus a "dark" exposure and a single bright or "flat" exposure to a uniform source provide sufficient information to correct the data. Both dark and flat accumulation times should be

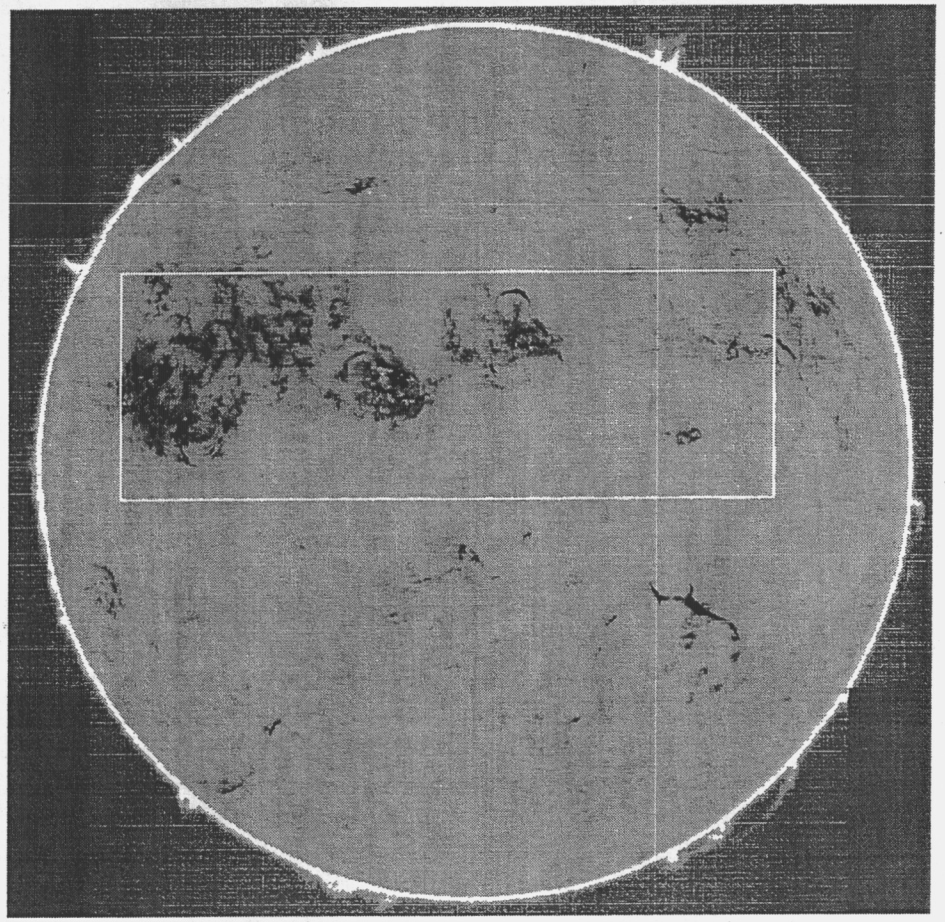

Figure 2. Synoptic, full-disk SPM He I 1083 nm equivalent width for 99 November 9. White rectangle marks area of subsequent zone area scan. Heliocentric north is at the top, west at the right.

considerably longer than that used for data acquisition so that the random noise added during the correction process does not significantly degrade the observations. Note that a single flat cannot correct non-linear detector response or unwanted temporal variations in the optical path or detector.

For a solar instrument, the Sun itself, which unfortunately for this purpose is spectrally and spatially non-uniform, is the only source bright enough to mimic observing conditions. Moreover, for spectroscopic observations, *any* change of the instrument to make the solar image appear more uniform (e.g., de-focusing the telescope, inserting optical diffusers, or rotating the grating to place nearby continuum on

the detector) also changes the fixed pattern, particularly the component due to interference fringes.

"Raw" flats for the SPM are obtained by scanning the solar image limb-to-limb parallel to the entrance slit while accumulating exposures so that each position on the slit has the same total exposure to sunlight. Assuming no temporal solar variations, a perfect optical and detector system would yield the same spectrum for every slit position. A raw flat for the zone area scan of 1999 November 9, with dark image subtracted, is shown in the upper left of Figure 3. No optical components except the mirror for spatial scanning are moved between obtaining the raw flat and the observations.

The fitting algorithm is based on the supposition that the raw flat has three components: (1) large-scale (of order the size of the spectral image) variations with no preferred orientation; (2) small-scale variations due to pixel-to-pixel gain variations, interference fringes, and optical contaminants such as dust, again with no preferred orientation in the camera frame; and (3) the averaged solar-telluric long-slit spectrum, the dispersion of which in our case is oriented along camera columns and varies over all scales. We wish to remove the spectral component (3) from the raw flat, since this is the object of interest in the observations, and to leave the components (1) and (2) in place so that they may be removed from the observations using the derived flat-field image. We separate these components with the following series of operations. Numbers for each step correspond to those underneath the relevant segment of Figure 3, with "0" denoting the trimmed raw flat.

1. Form an image of the large-scale intensity variations from low-order least-squares fits of intensity vs pixel position for each column (parallel to the dispersion), iteratively rejecting points 10 AD units below the current fit to select "continuum" points. The least-squares basis is a cubic spline with three equal segments.

2. Form a "detrended" flat by dividing the raw flat by the large-scale image of step 1. The result ideally contains only small-scale and spectral features.

3. Remove spectral features from the detrended flat by dividing it by least-squares fits to each image row (parallel to the slit). The result is ideally an image of the small-scale variations. The least-squares basis is a five-segment cubic spline, and all data points are included.

4. Form a "trial" flat by multiplying the small-scale (step 3) and large-scale (step 1) images. Spectral features are largely removed.

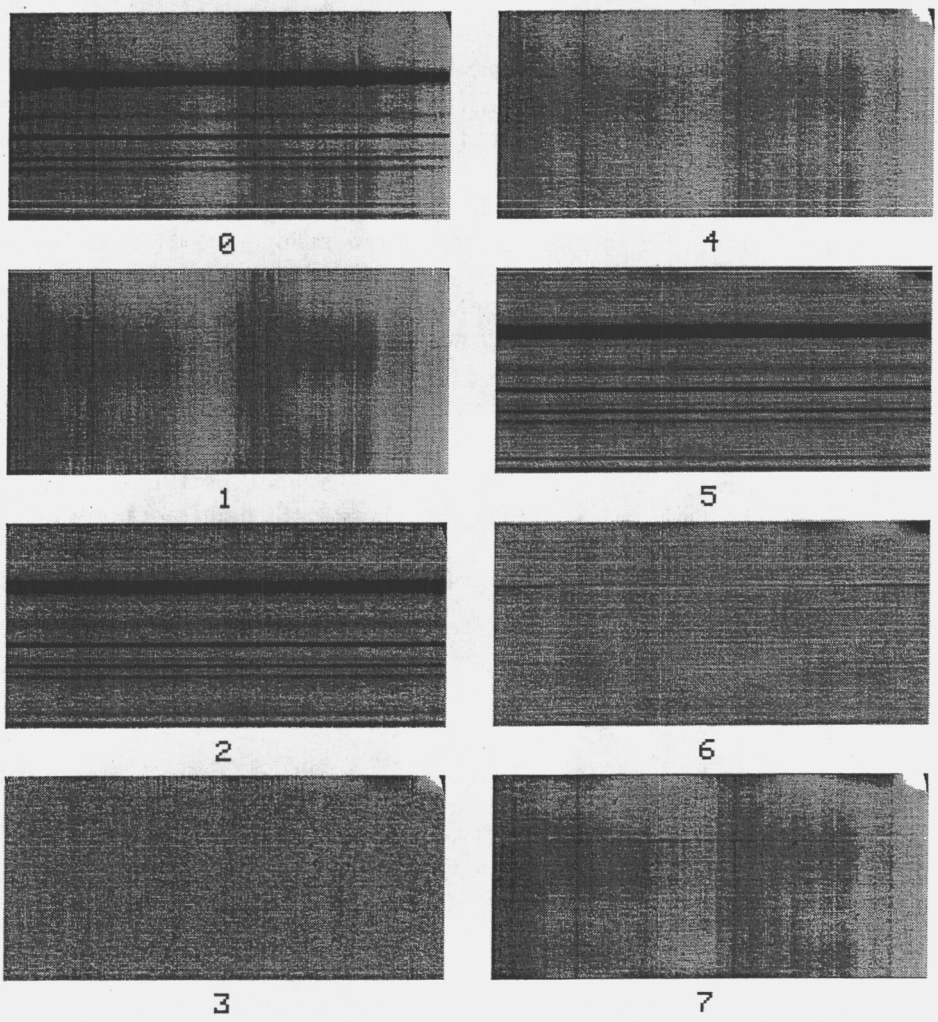

Figure 3. Fixed pattern removal; images are numbered according to the steps in the accompanying discussion, with 0 denoting the raw flat-field image after trimming to remove unused areas of the camera.

5. Form a trial "cleaned" flat by dividing the raw flat by the trial (step 4). If steps 1-4 were perfect, each column of the result would contain an identical spectrum. We enforce this condition on the final result with the following steps.

6. Form a corrector by dividing the clean trial (step 5) by its spatial (row) average.

7. Form the final flat by dividing the trial (step 4) by the corrector (step 6).

Steps 5-7 are not necessary for many purposes and are omitted, for example, when forming flat-field images for magnetograms. Experience has shown that the final corrections, which subtly alter continuum portions of the spectra, do help in the analysis of 1083 nm SPM data in areas where the line is weak. To compensate for curvature of the dispersion, each column of the trial cleaned flat (step 5) is shifted using the center of the telluric line as a reference before forming the spatial average in step 6, and the result is shifted in the reverse direction before forming the final flat in step 7. Notice that some evidence of the Si line is reintroduced in the final flat by this correction since the value of the dispersion also varies slightly with position along the slit. This defect has little effect on analysis of the He line and could probably be avoided by also using the Si line as a reference to dilate as well as shift the spectra. In this particular example, a small portion of the edge of the field lens is still visible in the upper right hand portion of the trimmed raw flat. This introduces mild oscillations in some of the least-squares procedures in portions of the spectra far enough removed from the 1083 nm line to have negligible effect on subsequent analysis.

4. Spectrum Analysis

Ordinarily, the 1083 nm spectra are analyzed to produce images of Doppler velocity, continuum intensity, equivalent width, central line depth, line asymmetry, and Doppler width for the He I line. The images for these quantities in the area outlined in Figure 2 as determined by the rapid analysis procedure described below are shown in Figures 4 and 5. In both figures, vertical tick marks show the slit positions for long-slit spectra with selected features labeled V (peculiar velocity feature), F, (flare with He I 1083 nm in true emission), H (coronal hole) and Q (quiet sun). The spectra themselves are shown in Figure 6 with slit direction vertical to correspond with the images in Figures 4 and 5 and wavelength increasing to the right. Finally, the spectral profiles at these four positions are plotted in Figure 7.

The most difficult quantity to determine is the continuum intensity which forms the reference for the rest of the spectral analysis. As mentioned earlier, small systematic or random errors in continuum determination are amplified in the normalized line profiles when the line is weak, and this problem is complicated by nearby telluric and solar lines with which the 1083 nm line is blended in proportions which vary markedly in space and time. The following procedure, samples of which are indicated by dashed lines in Figure 7, was developed by trial and error and seems to be reasonably accurate and robust. We begin

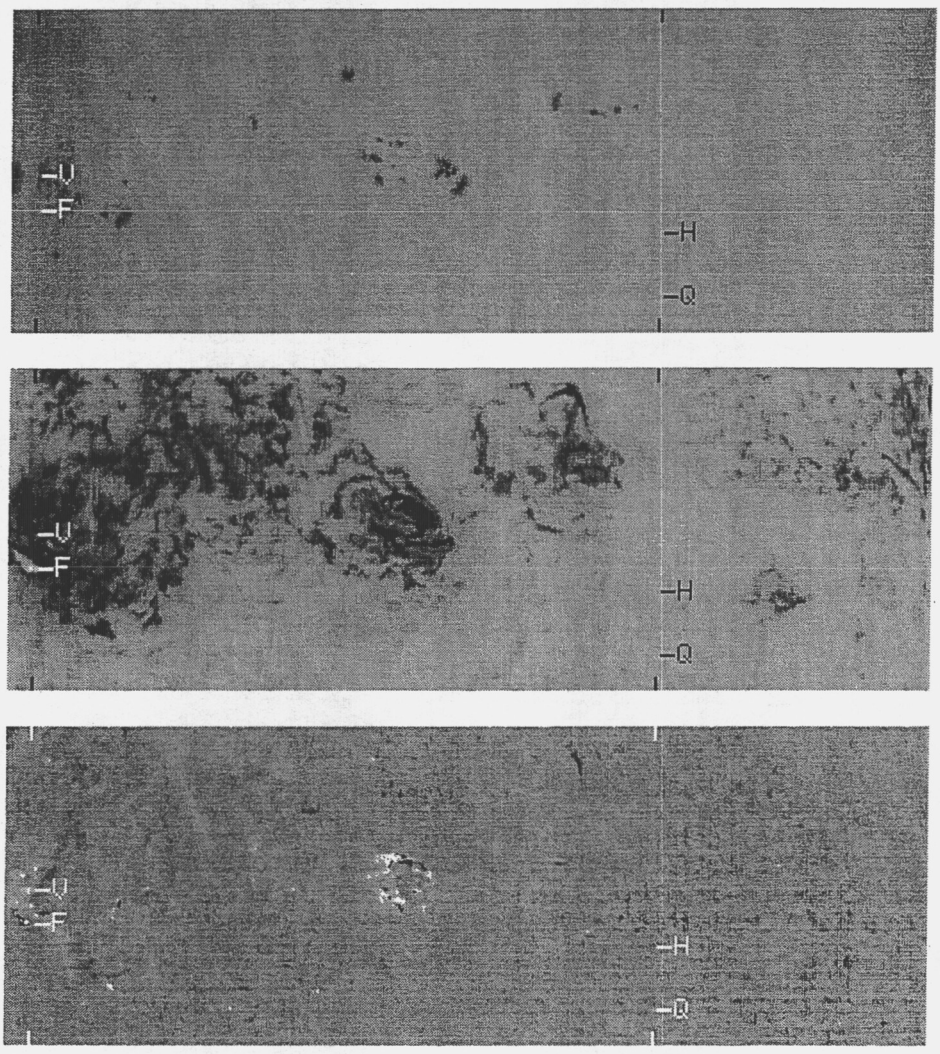

Figure 4. Intensity (top), equivalent width (middle – negative contrast), and asymmetry (bottom) for the zone area scan of 99 November 9.

by preselecting four spectral windows, which are marked in the sample spectrum of Figure 7, that appear to be free of spectrum lines at least when the 1083 nm line is weak and unshifted; one of these is on the blue side of the Si I 1082.7 line and another is to the red of the telluric-solar blend. A quadratic least-squares fit of intensity vs wavelength is passed through the measurements in these windows; intensities lying below the fit by an amount exceeding 0.001 of the average of the included data are rejected and the procedure is repeated until none of the data points from the previous iteration are rejected. This procedure tends to reject

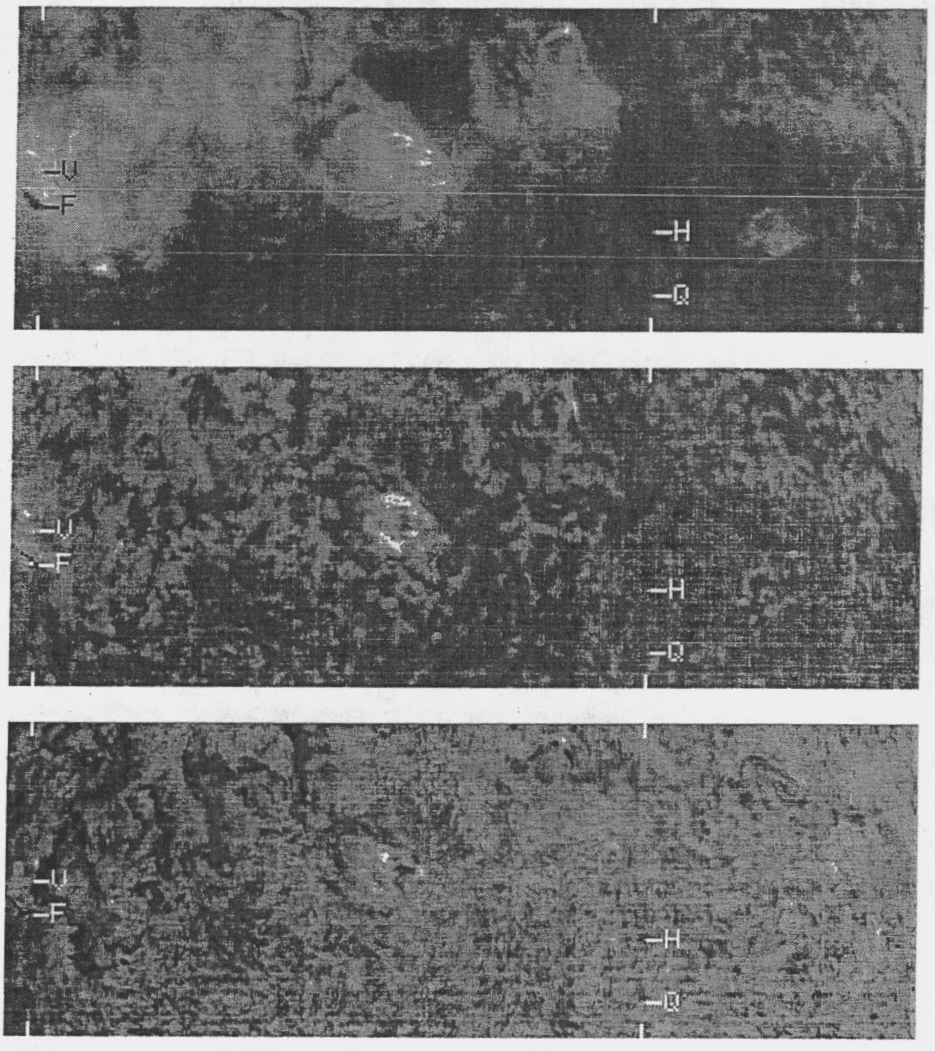

Figure 5. Line depth (top – positive contrast), Doppler width (middle), and Doppler velocity (bottom) for the zone area scan of 99 November 9.

continuum windows contaminated by Doppler shifts or variations in line strength for the 1083 nm line.

The continuum as determined above usually passes a little above the maximum intensities surrounding the 1083 nm line, mostly as a result of blending with the Si I line to the blue and the telluric water vapor line to the red. To compensate for these blends, we try to fit the two lines and remove them from the spectrum. The procedure begins by determining their line-center (maximum line depth, using the above continuum as a reference) wavelengths with the standard SPM algo-

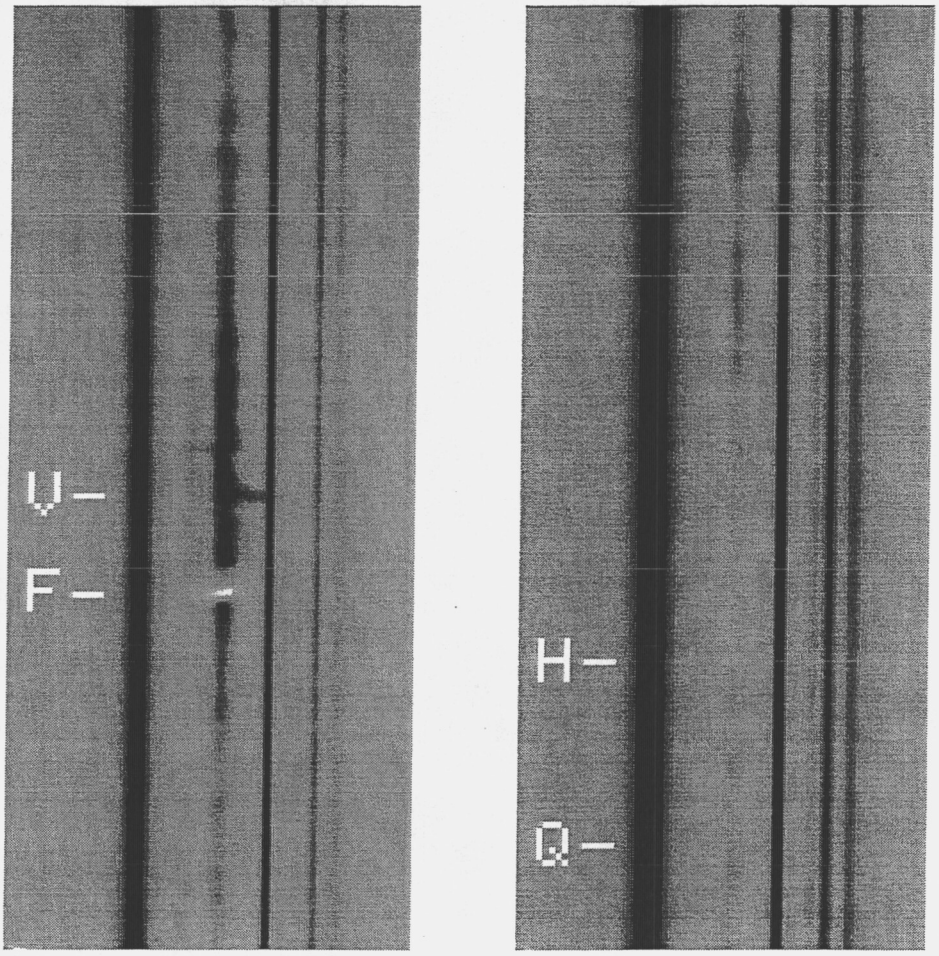

Figure 6. Long-slit spectra at the positions denoted by vertical tick marks in Figures 4 and 5.

rithm which searches for the zero of the convolution of the line profile with a pre-specified antisymmetric kernel (Jones *et al.*, 1992; Jones, 1996). The telluric line center also serves as a wavelength reference for the rest of the analysis.

A number of attempts were made to model the Si I 1082.7 nm and the telluric 1083.2 lines with least-squares fits of Voigt profiles. Although the residuals from these models tend to be small compared to the central line depths, systematic deviations in the wings are often comparable to the line depth of the He I line and can easily lead to 1083 nm equivalent widths of the wrong algebraic sign. A better approach is to fit the data empirically with least-squares splines. For the Si line, we take advantage of the fact that the blue wing is apparently free of

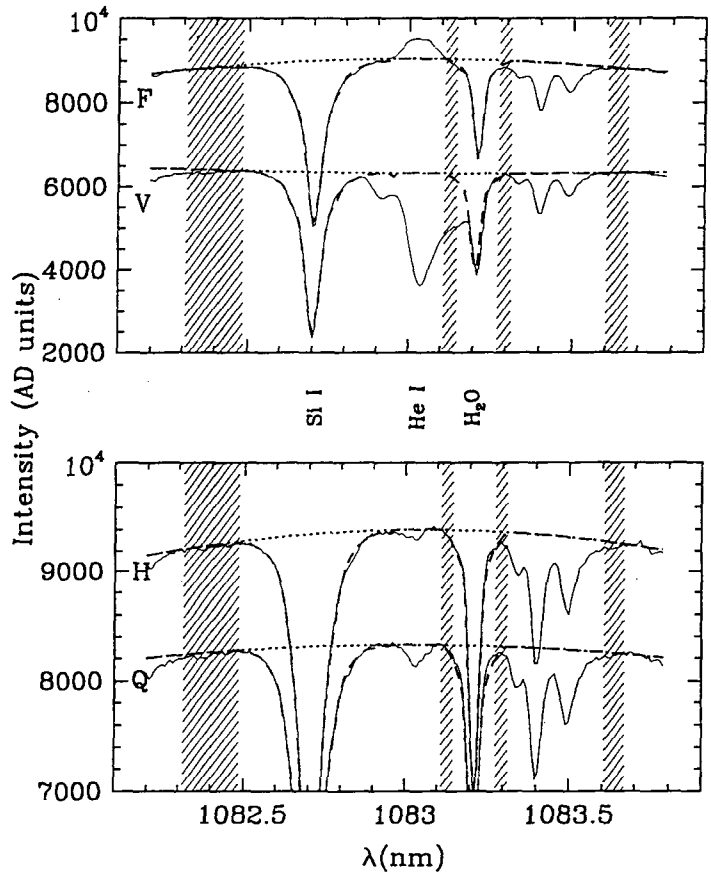

Figure 7. Intensity vs wavelength (solid line) for the spectral features marked in Figure 6. Shaded areas show wavelength zones for continuum determination, dotted curves show the continuum, and dashed curves show the fits to the Si I and telluric H_20 lines.

other spectral contaminants. Thus, we fit the entire line-depth profile with an 18-segment spline with prespecified knots designed to give a good representation of the data. We assume that the primary source of asymmetry in the wings of the Si line is the blend with the 1083 nm line. Thus the reflection of the blue wing about the measured line center (using the fitted spline as an interpolator) is taken as the best estimate of the Si profile were it the only absorber in the region; this symmetrized fit is added to the data to recover the "true" continuum in the absence of the Si line. There is often some trace of the line evident near the Si line center in this result, but this is usually well away from the spectral regions affecting the 1083 nm analysis.

A slightly different approach is used to remove the telluric line, since neither wing is reliably free of other absorbers. The underlying assumption for this analysis is that the line has an intrinsic profile whose width and depth is affected by the amount of water vapor and thermodynamic conditions along the line of sight. The shape of this profile as measured by the SPM was determined as the symmetrized spatial average of line depth profiles in a coronal hole near disk center where the 1083 nm line was particularly weak and appeared well separated from the telluric line. The central depth and full-width at half-maximum of the telluric line as measured at each spatial point (using the continuum as determined above) is then used to scale the reference profile to the actual conditions by spline interpolation. The data are divided by the transmission function resulting from this analysis to remove the affects of the telluric line. Fits to the Si and telluric lines are shown by dashed curves in Figure 7.

Once the deblended data, I^*, are computed as above, the analysis of the 1083 nm line is straightforward. The line depth is computed as

$$D(\lambda_i) = I_c(\lambda_i) - I^*(\lambda_i)$$

and the central wavelength such that $D(\lambda_0)$ is a maximum is found by the standard SPM algorithm discussed above. The Doppler velocity is then computed as

$$v_{||} = (c/\lambda_{lab})(\lambda_0 - \lambda_t - \Delta)$$

where c is the speed of light, λ_0 is the laboratory wavelength of the 1083 nm line, λ_t is the wavelength of the telluric line, and Δ is the average wavelength difference between the 1083 nm and telluric lines. The quantity $I_c(\lambda_0)$ is returned as the continuum intensity, and the equivalent width is simply calculated as

$$q = \delta\lambda \sum_i D(\lambda_i)/I_c(\lambda_i)$$

where $\delta\lambda$ is the wavelength subtended by one pixel and the sum is over a fixed number of pixels centered about λ_0. The central line depth relative to the continuum is

$$d = D(\lambda_0)/I_c(\lambda_0)$$

where D and I_c are evaluated at λ_0 by local cubic interpolation. Two wavelengths $\lambda^{\pm}$ are found from a cubic least-squares fit of intensity vs wavelength to the six points surrounding the interval where the line depth falls to $1/e$ of its maximum value, so that $D(\lambda^{\pm}) = D(\lambda_0)\exp(-1)$; the Doppler width in velocity units is then

$$\lambda_D = (c/\lambda_{lab})(\lambda^+ - \lambda^-)$$

while the asymmetry is defined as

$$a \equiv (c/\lambda_{lab})[(\lambda^+ + \lambda^-)/2 - \lambda_0].$$

Figure 8 shows the results of the above analysis for the four features marked in Figure 6. Intensity, normalized to the continuum and corrected for the Si I and telluric lines, is plotted as a function of wavelength near 1083 nm, and the intensities and wavelengths corresponding to λ_0 and $\lambda^{\pm}$ are marked. *Given the determination of continuum and blend corrections*, the above procedures place the line-center and $1/e$ profile points in reasonable positions with respect to the data for diverse profile shapes, even in the presence of considerable noise. Thus derived quantities in Figures 4 and 5 should accurately reflect the observed spectra.

5. Discussion

The images and spectra shown in Figures 4 - 7 were chosen to illustrate the variety and complexity of He I 1083 nm phenomenology. The flare (point F) which was in progress during this observation shows the He line in true emission, an infrequent event. The "velocity" event (point V) shows He absorption far enough redward of its ordinary spectral domain to become strongly blended with the telluric water vapor line. As can be seen in Figure 7, one of the fixed continuum zones is now entirely within the spectrum line. High velocity events are relatively common and are responsible for many isolated bright points seen in the synoptic full-disk images. Event V is spectroscopically similar to one of the time steps reported by Schmidt, Muglach, and Knölker (2000) and could well be another example of free-falling material. Even more extreme velocities are occasionally observed. Penn (2000), for example,

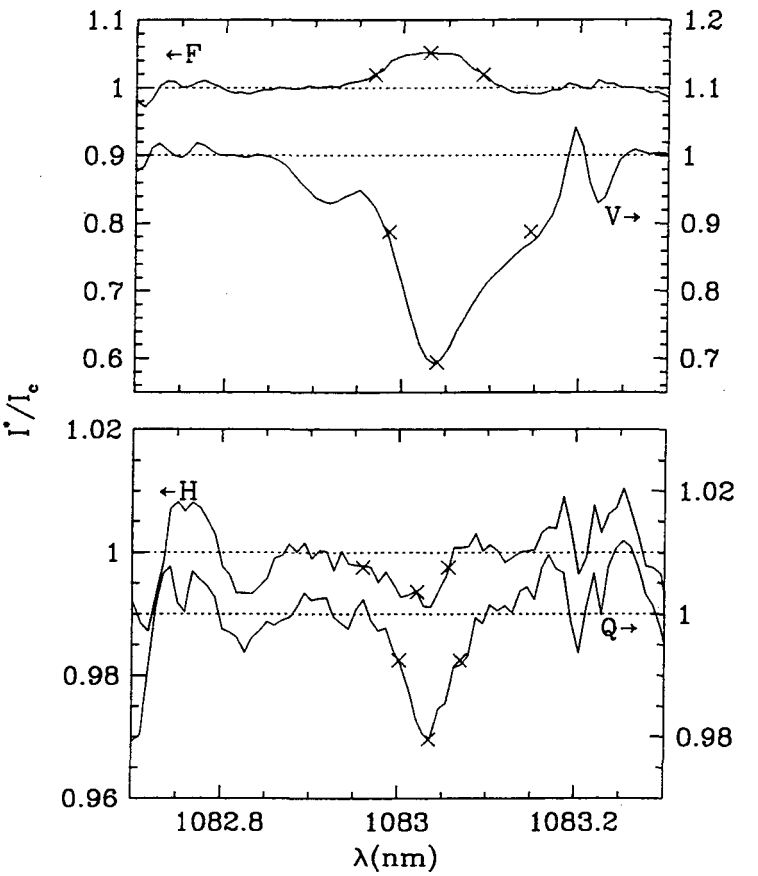

Figure 8. Deblended intensity normalized to the continuum vs wavelength for the spectral features marked in Figure 6. x's mark central and d/e wavelengths and intensities. Left and right arrows point to the appropriate intensity scales for each feature, and dotted lines mark the reference intensity level.

studied an erupting filament viewed with spectroscopic imaging where disjoint He absorption appears in the blue wing of the Si I line showing outflowing material with velocities of $\approx$ 300 km/s. The extreme variability shown in these features makes a general non-interactive analysis algorithm very difficult to devise.

Although less prominent, the much weaker absorption profiles in the quiet sun (e.g., point Q) and especially coronal holes (e.g., point H) are even more difficult to analyze accurately, since even the procedure for continuum extraction discussed above and illustrated in Figure 7 does not work uniformly well over an entire image. The equivalent widths of points Q and H are similar, but excess blueward absorption as noted by Dupree, Penn, and Jones (1996) is evident at point H. Such profiles have negative (dark in Figure 4) asymmetry as defined above and appear more frequently within coronal holes as can be seen in the lower part of Figure 4. However, quantitative determinations of both asymmetry and velocity are extremely sensitive to accurate placement of the reference continuum and are still at the limit of the procedures presented in the previous section.

Numerous observations similar to the one shown here have been collected since the SPM was placed into service, and more extensive analysis and interpretation of individual features or classes of features will be presented in separate papers. In addition, more refined analysis techniques using reference spectra as an aid to determining the continuum and full least-squares fitting over the entire observed spectral domain are being developed and will be reported separately.

Acknowledgments

The author wishes to thank summer research assistants W. Winters, S. van Damm, and C. Bender for assistance in developing the procedures and algorithms discussed here and V. Andretta, M. Penn, and E. Malanushenko for many useful discussions. This work was partially supported by NASA Office of Space Science Supporting Research and Technology grants 344-12-52-14 and 344-12-52-19. NSO/KPVT data used here were obtained cooperatively by AURA/NSO, NASA/GSFC, and NOAA/SEC.

References

Andretta, V., Del Zanna, G., and Jordan, S.D.: 2003, *Astron. Astrophys.*, in press.
Andretta, V. and Jones, H.P.: 1997, *Astrophys. J.* **489**, 375.
Dupree, A.K., Penn, M.J., and Jones, H.P: 1996, *Astrophys. J.* **467**, L121.

Janssen, P.J.C.: 1868, *Compt. Rend.* **67**, 839.
Jones, H.P.: 1996, in D.M. Rust ed., *Missions to the Sun*, SPIE Proceedings **2804**, 110.
Jones, H.P., Duvall, T.L. Jr., Harvey, J. W., Mahaffey, C.T., Schwitters, J.D., and Simmons, J.E.: 1992, *Solar Phys.*, **139**, 211.
Jordan, C.: 1975, *Monthly Notices Roy. Astron. Soc.* **170**, 249.
Jordan, C., Macpherson, K.P., and Smith, G.R.: 2001, *Monthly Notices Roy. Astron. Soc.* **328**, 1098.
Lin, H., Penn, M.J., and Kuhn, J.R.: 1998, *Astrophys. J.* **493**, 978.
Penn, M.J.: 2000, *Solar Phys.* **197**, 313.
Penn, M.J., Jones, H.P.: 1996, *Solar Phys.* **168**, 19.
Peter, H.: 1999, *Astrophys. J.* **522**, L77.
Schmidt, W., Muglach, K., and Knölker, M.: 2000, *Astrophys. J.* **544**, 567.
Solanki, S.K., Lagg, A., Woch, J., Krupp, M., and Collados, M.: 2003, *Nature*, submitted.

Address for Offprints: NASA's GSFC, Southwest Solar Station, c/o NSO, PO Box 26732, Tucson, AZ 85726